Paper accepted for publication in International Journal of Fatigue, 2006

Bump Extraction Algorithm for Variable Amplitude Fatigue Loading

S. Abdullah[1], J.C. Choi[2], J.A. Giacomin[3] and J.R. Yates[3]

[1]Dept. of Mechanical and Materials Engineering, Universiti Kebangsaan Malaysia, Bangi, 43600 UKM Bangi, Selangor, Malaysia.

[2]Hyundai Motor Company, South Korea.

[3]Dept. of Mechanical Engineering, The University of Sheffield, Mappin Street, Sheffield, S1 3JD, United Kingdom.

Abstract

This paper presents the development of a fatigue mission synthesis algorithm, called Wavelet Bump Extraction (WBE), for summarising long records of fatigue road load data. This algorithm is used to extract fatigue damaging events or bumps in the record that cause the majority of the fatigue damage, whilst preserving the load cycle sequences. Bumps are identified from characteristic frequency bands in the load spectrum using the 12th order Daubechies wavelet. The bumps are combined to produce a mission signal which has equivalent signal statistics and fatigue damage to the original signal. The WBE accuracy has been evaluated by observing the cycle sequence effects of the bump loadings. The WBE was compared with the time domain fatigue data editing method, so that the effectiveness of WBE can be verified. Using WBE, a substantial compression of the load-time history could be achieved for the purpose of accelerated fatigue tests in the automotive industry.

Keywords: fatigue data editing, mission, wavelet, bump, variable amplitude

[1] Corresponding author: Shahrum Abdullah (shahrum@vlsi.eng.ukm.my; mcabdul@yahoo.com); Tel: +60 – 3 – 89216511.

1. Introduction

Fatigue damage analysis is one of the key stages in the design of vehicle structural components. One of the vital input variables is the load history. For ground vehicles, these can cover an extremely wide range of uses and hence a representative road load time history is hard to quantify. By necessity, vehicle development requires accelerated fatigue testing and this is often accomplished by correlating test tracks with public road data. Both roads and test tracks generate variable amplitude (VA) load time histories [1]. For the laboratory fatigue test, VA loadings need to be edited by removing small amplitude cycles for reducing the test time and costs. Such a technique is known as fatigue data editing. Using this approach, large amplitude cycles that cause the majority of the damage are retained, and thus a shortened loading consists of large amplitude cycles is produced.

Several data editing techniques have been developed for use in the time domain [2]. Some computational algorithms were developed to omit the small amplitude cycles so as to retain the large amplitude cycles, such as: the application of the local strain parameter and linear damage rule in selecting the edit levels of VA loading while retaining the original history's sequence [3], the use of a nonlinear damage rule incorporating overstrain and sequence effect [4], the use of a damage window joining function to produce an edited signal [2,5] and the application of Smith-Watson-Topper (SWT) parameter to determine the range of low amplitude cycles that should be eliminated [6]. In the frequency domain, a time history is low pass filtered on the basis that high frequency cycles have small amplitudes which are not damaging [5].

Although high frequency cycles tend to be small in amplitude they are still superimposed on the lower frequency components and therefore add to the in order to contribute to the total fatigue damage. This filtering method does not shorten the signal, therefore the number of points of the edited loading is similar to the original loading. The time-frequency approaches have also been applied to the problem of fatigue data editing through its use in spike removal and de-noising [7].

Since the nature of significant fatigue damaging events must play a part in determining the degree of damage occurring, it seems appropriate to see a method to summarise road load data whilst preserving cycle sequence. It is proposed to explore a method based on the Mildly Nonstationary Mission Synthesis (MNMS) algorithm which was applied in vibration and comfort research [8-10]. Realising the MNMS algorithm is not suitable for fatigue studies [11], has led to the development of the Wavelet Bump Extraction (WBE) algorithm. The WBE algorithm is designed to identify and extract the fatigue damaging events, or bumps, from a VA road load time history to produce a shortened mission signal [12]. Consequently, it is important to maintain fatigue damage of the mission signal as close to the original signal, with the retention of the original load sequences.

2. Theoretical Background

2.1 Fatigue Life Prediction under VA Loadings

It is common that the service loads acquired on components of machines, vehicles, and structures are analysed for fatigue life using crack growth approaches. This approach is suitable for high capital valued structures, such as large aircraft, space shuttle, pressure vessels and oil rigs [1]. The ability to inspect for cracks and monitor their growth until a maximum allowable defect size is reached, enables the useful life to be extended beyond the original design life. However, it is not generally feasible for applying the crack inspection process for the inexpensive components that are made in large numbers. Applying periodic inspections on these components would generally increase the maintenance cost. Examples of components which fall in this category are automobile engine, steering and suspension parts [13]. For these components, it is important to predict crack initiation in order to avoid fatigue failure by replacing the part from service at the appropriate time.

A fatigue life estimation based on the related strain-based approach is usually used in these cases [1,14]. The strain-life fatigue model relates the plastic deformation that occurs at a localised region where fatigue cracks begin to the durability of the structure. This model is often used for ductile materials at relatively short fatigue lives. This approach is also can be used where there is little plasticity at long fatigue lives. Therefore, this is a comprehensive approach that can be used in place of the stress-based approach.

Current industrial practice for fatigue life prediction is to use the Palmgren-Miner (PM) linear damage rule. For strain-based fatigue life prediction, this rule is normally applied with strain-life fatigue damage models. The first strain-life model is the Coffin-Manson relationship, i.e.

$$\varepsilon_a = \frac{\sigma'_f}{E}\left(2N_f\right)^b + \varepsilon'_f\left(2N_f\right)^c \tag{1}$$

where E is the material modulus of elasticity, ε_a is a true strain amplitude, $2N_f$ is the number of reversals to failure, σ'_f is a fatigue strength coefficient, b is a fatigue strength exponent, ε'_f is a fatigue ductility coefficient and c is a fatigue ductility exponent.

Some of the realistic service situations involve non-zero mean stresses. Two mean stress effect models are used in the strain-life fatigue damage analysis, i.e. Morrow and SWT strain-life models. Mathematically, the Morrow model is defined by

$$\varepsilon_a = \frac{\sigma'_f}{E}\left(1-\frac{\sigma_m}{\sigma'_f}\right)\left(2N_f\right)^b + \varepsilon'_f\left(2N_f\right)^c \tag{2}$$

where σ_m is the mean stress. The SWT strain-life model is mathematically defined by

$$\sigma_{max}\varepsilon_a = \frac{\left(\sigma'_f\right)^2}{E}\left(2N_f\right)^{2b} + \sigma'_f\varepsilon'_f\left(2N_f\right)^{b+c} \tag{3}$$

where σ_{max} is the maximum stress for the particular cycle.

Several limitations were found in the implementation of the PM linear damage rule. Using this approach, the fatigue damage is accurately calculated for constant amplitude (CA) loadings, but it may lead to the erroneous prediction for VA loadings [15]. Considering the importance of sequence effects and the limitation of the PM linear

damage rule for analysing VA loadings, therefore, a suitable approach needs to be identified.

Several studies related to the fatigue life prediction on metal components were performed in order to solve the problem under VA loadings. For examples, a model derived from random vibration theory [16], non-linear damage summation models [17] and the fracture mechanics approach [18]. Even though these approaches gave better improvement, however, they were difficult to associate with fatigue life prediction programmes for general use. Therefore, a general strain-life fatigue damage model, or known as Effective Strain Damage (ESD) has been introduced [19]. This model is based on crack growth and crack closure that works well for a wide variety of materials, load spectra, component geometries, strain magnitudes and mean-strain effects. The model is mathematically defined as following

$$E\Delta\varepsilon^{*} = A(N_f)^{B} \tag{4}$$

where E is the elastic modulus of a material, $\Delta\varepsilon^{*}$ is a net effective strain range for a closed hysteresis loop that is related to fatigue crack growth. A and B are the material constants, and N_f is the number of cycles to failure. The magnitude of $E\Delta\varepsilon^{*}$ for a given cycle is a function of crack-opening stress, S_{op}, level and it is dependant on the prior stress and strain magnitudes in the loading history. The expression of $E\Delta\varepsilon^{*}$ can be expanded to

$$E\Delta\varepsilon^{*} = E\,(\varepsilon_{max} - \varepsilon_{op}) - E\varepsilon_i \tag{5}$$

where ε_{max} and ε_{op} is the maximum strain and the crack-opening strain of the particular cycle, respectively. ε_i is the intrinsic fatigue limit strain range under the VA loading condition. In order to consider the cycle sequence effects in the fatigue life calculation,

a decay parameter, *m*, is used to define the change in a crack-opening stress between two adjacent cycles. ΔS_{op} is defined as

$$\Delta S_{op} = m(S_{ss} - S_{cu}) \tag{6}$$

where S_{cu} is the current opening stress and S_{ss} is the steady-state opening stress. S_{cu} is defined as the S_{op} value of the previous cycle. S_{ss} is defined as the following equation:

$$S_{ss} = \alpha S_{\max}\left(1 - \left(\frac{S_{\max}}{S_y}\right)^2\right) + \beta S_{\min} \tag{7}$$

where α and β are the material constants, S_{max} is the maximum stress of the previous largest cycle in the time history, S_{min} is the minimum stress of the previous largest cycle and S_y is the cyclic yield stress.

2.2 Wavelet Transforms

Many experimental signals exhibit time-varying, or nonstationary characteristics, which provide a challenge in signal analysis [21]. Traditional approach for the frequency domain analysis of the time series was performed using the Fourier transform. This kind of analysis is not suitable for nonstationary signal, as it cannot provide any information of the spectrum changes with respect to time [22]. Realising the limitation of the Fourier transform for nonstationary signals, therefore the wavelet transform is more suitable. The wavelet transform is the functions in the time-scale domain and it is a significant tool for presenting local features of a signal. The wavelet transform gives a separation of components of a signal that overlap in both time and frequency and it gives a more accurate local description of the signal characteristics. Using the wavelet domain analysis, the time and frequency of an oscillating signal can be detected [23].

Wavelets are analytical functions $\psi(t)$ which are used to decompose a signal $x(t)$ into scaled wavelet coefficients $W_\psi(a,b')$. The continuous wavelet transform is a time-scale method that can be expressed as

$$W_\psi(a,b') = \frac{1}{\sqrt{a}} \int_{-\infty}^{\infty} x(t)\psi^*\left(\frac{t-b'}{a}\right) \mathrm{d}t \tag{8}$$

where $\psi_{a,b}(t)$ are the scaled wavelets and ψ^* is the complex conjugate of ψ. The basis wavelet $\psi(t)$ can be chosen from a number of functions which satisfy a set of admissibility conditions. The admissibility conditions is mathematically defined as

$$\int_{-\infty}^{\infty} \frac{|\Psi(\omega)|^2}{|\omega|} d\omega = C_\psi < \infty \tag{9}$$

where $\Psi(\omega)$ is the Fourier transform of the mother wavelet. This condition is used for the inversion process of the wavelet transform.

A natural extension of continuous analysis is the discretisation of time *b'* and scale *a* according to $a = a_0^{\,m}$, $b' = na_0^{\,n}b_0$ where *m* and *n* are integers, $b_0 \neq 0$ is the translation step. This implies the construction of a time-scale grid, and thus a discrete wavelet transform can be defined by

$$W_\psi(m,n) = \int_{-\infty}^{\infty} x(t)a_0^{\,-m/2}\psi^*\left(\frac{t-nb_0a_0^{\,m}}{a_0^{\,m}}\right) \mathrm{d}t \tag{10}$$

When the wavelets $\psi_{m,n}(t)$ form a set of orthonormal functions there is no redundancy in the analysis, i.e. the procedure can be precisely inverted. The discrete wavelet transform based on such functions is called the Orthogonal Wavelet Transform (OWT).

There are many wavelet families and one of the most famous is the Daubechies [24] that has the orthogonal basis functions. It is the discrete wavelet transform that allows the decomposition and reconstruction of the input signal in order to observe the signal

characteristics within the specific frequency band. Various applications of the orthogonal wavelet transform can be found in previous studies, such as in the application using nonstationary signals for the mechanical damage detection [25], the signal compression and de-noising process [26] and the application of MNMS for the comfort and vibration cases [8-10,27]. This transform was also performed in a fatigue study, i.e. the compression of nonstationary signals measured from a light railway train component [7] and the automobile data sets [11].

3. Development of the Wavelet Bump Extraction (WBE) Algorithm

A flowchart describing the WBE processing is presented in Fig. 1 and three main stages can be observed: the wavelet decomposition process; the identification and extraction of fatigue damaging events; and the construction of a mission signal.

INSERT FIG. 1

The first stage of the WBE algorithm is to calculate the power spectral density (PSD) of the input signal to determine its frequency domain characteristics. A PSD is used to convert a signal from the time domain to the frequency domain using the fast Fourier transform (FFT) method. To convert a time domain signal into the frequency domain, the signal is separated into a number of discrete sinusoidal waves of varying amplitude, frequency and phase. The FFT forms a complex vector of values which each value represents the amplitude and phase of the particular sinusoidal wave at a particular frequency. In the relation of the PSD with the FFT, the PSD is a normalised density plot

describing the mean square amplitude of each sinusoidal wave with respect to its frequency. The PSD is mathematically defined as the Fourier transform of its auto-correlation function.

An example of the PSD plot is shown in Fig. 2 which illustrate the distribution of the signal vibrational energy across the frequency domain. In this figure, the time history was transform into the frequency domain using the FFT in order to obtain its PSD distribution. In this PSD plot, each frequency step value is characterised by amplitude, A_k, as following equation

$$A_k = \sqrt{2\Delta f \cdot S(f_k)} \tag{8}$$

where $S(f_k)$ is underlying PSD of the Gaussian signal and f_k is the harmonic frequency. In the WBE algorithm, the PSD is applied in the wavelet grouping process of the input signal.

INSERT FIG. 2

Using the orthogonal wavelet transform, the 12th order Daubechies wavelet was chosen as the main wavelet function to decompose the input signal into the respective wavelet levels. The 12th order representation was adopted because of its successful application in several previous studies involving automotive road data [8-11,27]. Since Daubechies' wavelets of order N provides $\frac{N}{2}-1$ vanishing moments, the 12th order Daubechies wavelet is adequate for the WBE application since greater than two vanishing moments

are rarely required when compressing speech or video signals which these signals are more complex compared to a road load time history [28].

Wavelet decomposition process is equivalent to a multiple band-pass filter bank, dividing the vibrational energy of the original signal amongst the wavelet levels. Each wavelet level describes the time behaviour of the signal within a specific frequency band. The wavelet levels corresponds to a certain frequency range and retains all time domain features related to the transient events in the original road data. The wavelet levels are then grouped in such a way that each group isolates a single frequency band of the whole PSD. Following this logic, some groups will combine several wavelet levels while others may consist of only one individual wavelet level. Each wavelet group is defined by the user to cover frequency regions of specific interest such as high energy peaks caused by a subsystem resonance. This subdividing of the original signal (Fig. 3) permits analysis to be performed for each frequency region independently.

INSERT FIG. 3

In the second stage of WBE, fatigue damaging events, or bumps, are identified in the each wavelet group. A bump is defined as an oscillatory transient which has a monotonic decay envelope either side of a peak value. Bump identification is achieved in each wavelet group time history by means of an automatic trigger level that is specific to the wavelet group.

At the program launch (as illustrated in Fig. 1 and 2), the user is asked to specify initial trigger level values for each wavelet group. Trigger level determination is performed by specifying the percentage value of the peak for the wavelet group, which is denoted as *C1*. The user is also asked to specify the trigger step, which is denoted as *C2*, which is a percentage value which can be applied to the peak of each wavelet group. In addition, the user is asked to specify an acceptable percentage difference between the root-mean-square (r.m.s.) and the kurtosis of the mission signal and the original signal (denoted as *RD* and *KD*, respectively). Both statistical parameters are used in order to retain a certain amount of the signal vibrational energy and amplitude range characteristics.

The trigger level for each wavelet group is automatically determined to achieve the requested statistics (simultaneous analysis for both *RD* and *KD*) for each wavelet group. Referring to the flowchart of Figure 3.2, other parameters used in the WBE algorithm are *D1* and *D2*. Both parameters are defined as the calculated difference of r.m.s. (for *D1*) and kurtosis (for *D2*) between a current iteration of the mission signal and the original signal.

In the stage of identifying the trigger level value for each wavelet group, the simultaneous comparison between the values of *D1* with *RD* and the values of *D2* with *KD* are required. If the values of *D1* and *D2* are not found in the ranges of $\pm RD$ (or $-RD < D1 < +RD$) and $\pm KD$ (or $-KD < D2 < +KD$), respectively, the algorithm will then compute the trigger level step (*C2*) in order to calculate for a new trigger level value. This process is iterated until *D1* and *D2* meet the user-defined value of both *RD* and *KD*, thus the final trigger levels can then be finalised.

Since the WBE algorithm tends to retain signal energy and signal amplitude range in the experimental road load data, the use of ±10% difference in r.m.s. and kurtosis of the mission and the original signal is suitable. The percentage value of ±10% is chosen for the bump identification process in order to produce a shortened mission signal which has close global statistical parameter (PSD, r.m.s. and kurtosis) values to those of the original signal. Related studies of the difference in the global signal statistical values between the mission and the original signals using the experimental road load data sets can be found in related literature [10,11], with the application of the Mildly Nonstationary Mission Synthesis (MNMS) algorithm.

Fig. 4a presents a set of possible trigger levels for an individual wavelet group to determine a bump. Bump identification is performed by means of a search which identifies the points at which the signal envelope inverts from a decay behaviour. The two inversion points, one on either side of the peak value, define the temporal extent of the bump event and are shown in Fig. 4b.

INSERT FIG. 4

After all the bumps are identified in the respective wavelet groups, a method of searching the bump start and finish points from the original time history has been introduced (Fig. 4c). This is the final stage of the WBE algorithm, which is performed to extract bump segments from the original signal. If a bump event is found in any of the wavelet groups a block of data covering the time frame of the bump is taken from the original data set, retaining the amplitude and phase relationships of the original

signal. Since the bump segments are extracted based on the statistically determined trigger level values, these segments retain higher amplitude range and should create the majority of fatigue damage. Finally, the bump segments are sorted in the order of the original bump segment sequences to produce a mission signal.

4. Application of the WBE Algorithm

Two test signals have been applied with WBE for the purpose of algorithm validation. A synthetic test signal, named as T1 (see Fig. 5a), was defined with 16,000 data points and sampled at 400 Hz. The logic of creating T1 was to observe the ability of the algorithm to deal with any signal containing large transients in a small amplitude background, so that the bump events can be properly identified. This signal consists of a combination of sinusoidal and random signals of various amplitudes and frequencies, and it was intentionally defined to be a mixture of both high amplitude events and low amplitude harmonic background. The second, named as T2 (see Fig. 6a), is a fatigue strain signal that was measured on the lower suspension arm of a vehicle travelling at 34 km/h over a pavé test track. It was sampled at 500 Hz for a total of 23,000 data points that produced a total record length of 46 seconds. This signal exhibits a slight change in mean of the whole signal with a little low frequency content. This data set was chosen because it contained many small amplitude and high frequency bumps in the signal background.

INSERT FIG. 5

INSERT FIG. 6

Using the WBE algorithm, the signals were decomposed into the wavelet levels and the levels were then grouped into the particular frequency bands. T1 was decomposed into 11 wavelet levels and four wavelet groups were formed. T2 was decomposed into 12 wavelet levels that were assembled into four wavelet groups. The wavelet group time histories are shown in Fig. 5b for T1 and Fig. 6b for T2. For both data sets, Wavelet Group 1 and Wavelet Group 4 exhibit the low and high frequency data distribution, respectively.

In order to identify the bumps, trigger level values were set based on the r.m.s. and kurtosis difference between the original and mission signals. For this case, the ±10% difference in r.m.s. and kurtosis of the mission and the original signal was used for analysing experimental road load data sets. This is important in order to retain the signal energy and amplitude ranges [10,11]. Therefore, the shortened mission signal produced by the WBE algorithm has approximately the same global statistical values (PSD, r.m.s. and kurtosis) to those of the original signal.

For T1, the bump events cannot be properly extracted at the ±10% statistical difference. For this signal, the bumps were extracted using a ±75% difference in r.m.s. and kurtosis between the original and the mission signals. A large difference in r.m.s. and kurtosis values was required in the case of signal T1 as approximately 75% of the original signal contained low amplitude cycles, which significantly contributed to the r.m.s. and kurtosis calculations. Finally, T1 is also used to show the appropriate high amplitude events being extracted from the original time history, see Fig. 5b. For T2, a ±10% statistical difference was used in order to produce a mission signal which has equivalent

signal statistics to the original signal. High amplitude events are slightly difficult to quantify due to the signal being measured on the pavé surface, which includes many high energy impacts. The right side of Fig. 5b for T1 and Fig. 6b for T2 show high amplitude events were identified in each wavelet group.

The identified bumps in the wavelet groups of T1 (Fig. 5b) and T2 (Fig. 6b) show different bump patterns in terms of their frequency content were observed in lower frequency band (Wavelet Group 1) and higher frequency band (Wavelet Group 4). The bump in Wavelet Group 1 exhibits a decay enveloping of the transient shape as it has a longer time length. For Wavelet Group 4, it is difficult to observe the bump decay shape. It is due to the bump the time extent became shorter in the higher frequency wavelet group. From this observation, it is suggested that a bump in lower frequency band influences to the length of the bump segment and the mission signal.

Using a method of searching the bump start and finish points as introduced in Fig. 4c, the extracted bump segments are shown in Fig. 5c for T1 and Fig. 6c for T2. In these figures, all bump segments were located at their original position in the original signals. Fig. 5c shows that the correct high amplitudes were extracted from T1. For T2, nine bump segments were extracted from the original time history. In order to produce the WBE mission signal, these extracted bump segments were assembled together in order to produce a shortened time history, or called a mission signal, as illustrated in Fig. 5d for T1 and Fig. 6d for T2. In terms of time compression, the T1 mission signal is 12.5 seconds and 31.3% of the original signal. For T2, the length of the mission signal is 18.8 seconds and 40.9% of the original signal.

5. Experimental Stages

5.1 Determination of the Material Properties

Experiments were performed to determine the mechanical properties of the chosen material, hence to validate the WBE algorithm. Material properties which can be determined from experiments were monotonic mechanical properties from a tensile test and cyclic mechanical properties from uniaxial CA loading fatigue tests. The experimental CA data were used to define the parameter of strain-life models.

The material chosen for the test samples was BS 080A42 steel and often used in the suspension components of passenger cars. Specimens (see Fig. 7 for the geometry) were manufactured as an hourglass profile round bar for tension-compression loading which complied with ASTM E606-92 [29]. They were hand polished using several grades of silicone carbide abrasive paper and finished with 6-μm diamond compound. An Instron 8501 servo-hydraulic test machine was used in displacement control mode for all tests.

INSERT FIG. 7

A tensile test was performed to obtain the monotonic properties. Using this test the values of modulus of elasticity, the ultimate tensile strength and the 0.2% static yield stress were found to be at 210 GPa, 624 MPa and 342 MPa, respectively. The detail monotonic properties of BS 080A42 steel are listed in Table 1. Stress and strain data from nine different strain amplitudes of CA loading fatigue tests were used to plot the

strain-life curve, as illustrated in Fig. 8a. The parameters of the Coffin-Manson relationship were also tabulated in Table 1. Data in this table were then used to define the strain-life models of Eq. (1) – Eq. (3).

INSERT FIG. 8

INSERT TABLE 1

In order to observe the cycle sequence effects in the WBE processing, uniaxial fatigue tests of VA loadings were performed using the experimental signal of T2. Nine bump segment loadings of T2 (see Fig. 6c) were used for the uniaxial VA loading fatigue tests. Details of time position of these segments were listed in Table 2, showing B6 is the longest bump segment at 4.6 seconds and B2 is the shortest bump segment at 0.2 seconds.

INSERT TABLE 2

5.2 Determination of the Parameters for Fatigue Damage Model

The parameter values of Table 1 were used to define the parameter in Coffin-Manson, SWT and Morrow relationships, see Eq. (1) – Eq. (3). For the ESD model, Eq. (4), the parameter values of the material constants A and B were determined from the CA fatigue test data. A relationship between damage stress range ($E\Delta\varepsilon^{*}$) versus cycles to failure is plot as in Fig. 8b. The material constants of A = 119,000 MPa and B = –0.5

were determined using a linear regression curve fitting of the CA loading fatigue test data, resulting the final expression of Eq. (4) is

$$210000\ (\Delta\varepsilon^{*}) = 119000\ (N_f)^{-0.5} \quad (9)$$

The values of S_i (from $E\varepsilon_i$) in Eq. (5), m in Eq. (6), and α, β in Eq. (7) were used to calculate the value of $\Delta\varepsilon^{*}$. If there is no experimental data to help determine S_i, it can be inferred from the graph of fatigue intrinsic limit versus modulus of elasticity [30]. Using this graph, it gives the approximate S_i value at a particular value of modulus of elasticity, E. The values of α and β were determined using the experimental data of crack opening stress versus maximum stress [31]. The m value was determined from a curve fitting using the experimental data of crack opening stress against number of cycles [32]. For this study, no experimental data was available to determine the m, α and β values. Since the main objective of this research was to develop the fatigue data editing algorithm associated with cycle sequence effects, the measurement for determining these three parameters under VA loadings was not undertaken. Therefore, the m, α and β values were assumed from related studies on other carbon steels.

Previous works using SAE 1045 steel [19,31,32] showed that different values of α and β had been used for the ESD strain-life model. These values are then being used in the analysis of this paper in order to observe the sensitivity of the ESD model using different values of α and β when calculating the fatigue life.

Table 3 presents the fatigue lives obtained using different values of α and β (for SAE 1045 steel) for the original and the mission signals of T2. It can be seen that there were no changes in fatigue life (for T2 and its mission signal) with different values of α and β. The finding of this analysis suggested that the α and β parameters were not a major factor in the fatigue life prediction when using the ESD model. From the latest research of this model [32] using SAE 1045 steel which is a carbon steel, the values of *m*, α and β were 0.002, 0.55 and 0.23, respectively. Since BS 080A42 is also a carbon steel, therefore, the *m*, α and β values of SAE 1045 steel were used in this study.

Fig. 8c shows the comparison of the strain-life curves using the ESD model and the Coffin-Manson relationship. Both the ESD and Coffin-Manson strain-life curves have a close correspondence to the experimental data. From this comparison, it is concluded that the ESD strain-life model is also suitable for the fatigue life calculations.

In order to calculate the fatigue life of a VA loading using the ESD model, which the results were presented in Table 3, this loading was reconstructed based on the original load sequences in the time history. The time history reconstruction process is needed in order to associate the use of strain-life fatigue prediction method with cycle sequence effects. In the calculation, the time history was rainflow counted [34] for the extraction of the fatigue cycles. These cycles were then sorted based on the original peak-valley sequences in order to produce similar sequences as the original time history. For example, a reconstructed cycle history is shown in Fig. 9 for the first bump segment (B1).

INSERT FIG. 9

6. Results and Discussions

6.1 Which Strain-life Model for the WBE Algorithm?

The results of fatigue life determined using VA loadings were tabulated in Table 4. Parameters in Table 1 were used to predict the fatigue lives based on the Coffin-Manson, Morrow and SWT, and the prediction results were also tabulated in Table 4. In this table, the ESD fatigue lives of the eleven VA loadings using the parameters determined in the Section 5.2.

INSERT TABLE 4

The experimental uniaxial fatigue lives were compared with the predicted values (Table 5). Fig. 10 shows the correlation of fatigue lives between experiment and all four strain-life models. Each data point represents a loading condition in Table 4. The correlated fatigue lives between the ESD model and experiments were distributed around the 1:1 line and within the range of ± a factor of 2. However, the correlation points produced from three other strain-life models (Coffin-Manson, Morrow and SWT) were located outside the range of ± a factor of 2. It shows that there were close correspondences between the predicted fatigue lives using the ESD model and the experimental fatigue lives.

INSERT FIG. 10

From the results in Table 4, the average difference of fatigue life between the Coffin-Manson, Morrow and SWT strain-life models to the respective experimental results is 358%, 333% and 580%, respectively. Using the ESD model, the smallest difference was found to be of 17%. The results show a better accuracy of the ESD model to predict the fatigue lives of VA loadings compared to Coffin-Manson, Morrow and SWT models. The analysis of the experimental and analytical results using the T2 bump segments show a better accuracy for the ESD model to predict the fatigue lives of VA fatigue loadings compared to other strain-life models.

Based on the literature review, the ESD model was identified as a solution for fatigue life prediction using VA loadings. However, it is also important to validate the WBE algorithm with the fatigue life calculation using the established strain-life model for CA loading cases, i.e. the Coffin-Manson, Morrow and SWT strain-life models. The analysis using these three CA-based strain-life models, however, produced an overestimation in the fatigue life prediction when compared to the experimental results. This fatigue life overestimation occurred because of the use of these three strain-life models with the Palmgren-Miner linear damage rule which do not account for load interaction effects in the VA time histories. Since the ESD model has been developed [19] to solve the problem in fatigue life prediction under VA loadings, a close correlation (refer to Fig. 10) and the smallest difference (refer to Table 4) between this prediction and experimental results were expected to be produced from the research of this paper.

Considering the smallest fatigue life difference between predictions and experiment was found in the ESD model (17%), finally, it is concluded that the ESD model is the most suitable to predict the fatigue damage of VA loadings. The combination of ESD and WBE provide a novel development of the wavelet-based fatigue data editing technique with the extraction of bump segments or fatigue damaging events, and the preservation of the original load cycle sequences.

6.2 Comparison between WBE and the Time Domain Editing Technique

Since the WBE algorithm is a new fatigue data editing technique, it is important to compare this technique with an established procedure. According to research by El-Ratal *et al.* [2], the time domain fatigue data editing was recommended for accelerated fatigue tests, as the phase and amplitude of the original signal was retained in the shortened signal. The time correlated fatigue damage (TCFD) method, which was performed using nSoft® software package, was acknowledged as the technique applied [2] for editing VA fatigue loadings. Hence, this was used to compare with the WBE algorithm. TCFD is used to remove non-damaging sections of the time history on the basis of time correlated fatigue damage windows of the input signal. Windows with low amplitude cycles which contained minimal fatigue damage were removed. Using this approach, both the percentages of damage retention and the required acceleration factors, or one of them, could be set as editing targets [35].

In order to have the TCFD compressed signals at the similar time-length to the T2 mission signal, the original signal were reduced at 40.9%. This allowed the value of

2.45 to be as an acceleration factor for TCFD. In addition, the original fatigue damage was preserved at 100% for this signal. Fig. 11a shows the signals at similar time length which were obtained using the WBE algorithm and the TCFD method.

INSERT FIG. 11

The signals produced from WBE and TCFD were compared according to the r.m.s. value, the kurtosis value and the PSD plot. The r.m.s. and kurtosis comparison were chosen for their ability to characterise a random signal, and the frequency distributions in PSD were selected in order to observe the vibrational energy distribution of the time series. The comparison results are tabulated in Table 5, which WBE produced the signal with the r.m.s. and kurtosis closest to the original signal when compared to TCFD. The differences were found to be at 0.6% and 5.9% for the r.m.s. and kurtosis values, respectively. At this time compression and small differences in global signal statistical parameters between the edited and original signal gave an indication of the WBE effectiveness in the fatigue data editing application.

INSERT TABLE 5

In terms of PSD distribution in Fig. 11b, it is difficult to judge the difference between these two methods. At higher frequencies, a similar pattern of PSD can be found in both WBE and TCFD edited signals. The dissimilarity of these two edited signals was presented at lower frequency distribution. In Fig. 11c, a significant difference of low frequency content between the WBE mission signal and the TCFD compressed signal is

observed, especially in the frequency range of 0-1 Hz. The low frequency content of the T2 original signal was preserved in the WBE mission signal, but not for the TCFD compressed signal.

Considering better results were observed in the analysis of the WBE mission signal of T2, it is suggesting that the WBE algorithm is a better approach compared to TCFD. In order to strengthen this remark, the authors proposed further experimental studies are needed for improving the suitability of WBE for the fatigue data editing application. In addition, a comparison study between WBE and other fatigue data editing methods would also be useful.

6.3 WBE for an Accelerated Fatigue Tests

Using WBE as a fatigue data editing technique, the mission signal of T1 was 31.3% (12.5 seconds) of the original signal. At this record length, the mission signal retained 100% of the original fatigue damage, see Table 6. The fatigue damage or fatigue life values were calculated using the ESD model, considering the lowest average difference of the ESD results to the experiment was obtained, as in Section 6.1. For T2, the mission signal length was 40.9% (18.8 seconds) of the original signal. At this length, 100% of the original fatigue damage was retained in the mission signal, see Table 6. With these results, it indicates that the WBE algorithm is suitable for a fatigue data editing technique.

INSERT TABLE 6

Fig. 12 shows the fatigue life correlation between the WBE mission signals and the respective original signals using all strain-life fatigue damage models. In the figure each data point represents a loading condition from Table 6. The correlated fatigue lives between the ESD model and experiments were distributed around the 1:1 line and within the range of ± a factor of 2. These findings suggested that the closeness of the fatigue life of the mission signal to the original signal. It shows the acceptability of the mission signals to be used for accelerated fatigue tests. In this study, finally, the ability of WBE to shorten VA loadings by more than half their original length, while simultaneously retaining 100% of the original fatigue damage in the respective mission signal would be expected to prove useful for accelerated fatigue tests.

INSERT FIG. 12

7. Conclusions

This paper has discussed on the development of the new wavelet-based fatigue data editing algorithm, known as Wavelet Bump Extraction (WBE). This algorithm was designed for the purpose to extract fatigue damaging events or bump segments from a VA loading so as to produce a shortened or mission loading which preserves the original load sequences. Several concluded remarks can be pointed out based on the findings of this research:

1. The WBE algorithm is identified as the first wavelet-based for shortening a VA loading with an approach of removing low amplitude cycles which produced little or no damage.

2. Using the WBE algorithm, the mission signal retains the majority of the original amplitudes, load cycle sequences within the fatigue damaging events, fatigue damage and the vibrational energy of a signal.
3. Using the experimental T2 signal as a case study of this research, the fatigue damaging events were extracted at the ±10% r.m.s. and kurtosis difference between the mission and original signals. The value of ±10% was chosen for the bump identification process in order to produce a shortened mission signal which has close global statistical parameter (PSD, r.m.s. and kurtosis) values to those of the original signal.
4. Based on the relationship between the prediction and experimental results, a closer correspondence was observed when using the ESD model. Therefore, it is suggested that this model was found to be a suitable approach to predict fatigue lives using VA loadings.
5. A good fatigue life correlation between the WBE mission and original signals was observed. It shows that the suitability of the WBE mission signals for accelerated fatigue tests.

Acknowledgements

The authors wish to express our gratitude to Universiti Kebangsaan Malaysia, The University of Sheffield and Hyundai Motor Company for the support given for this research work. Many thanks to Leyland Technical Centre for providing vehicle data measured on the road surfaces.

References

[1] Dowling NE. Mechanical Behaviour of Materials: Engineering Methods for Deformation, Fracture and Fatigue. Second Edition, Prentice Hall, New Jersey, 1999.

[2] El-Ratal W, Bennebach M, Lin X, Plaskitt R. Fatigue life modelling and accelerated test for components under variable amplitude loads, Symposium on Fatigue Testing and Analysis Under Variable Amplitude Loading Conditions, 10th Int Spring Meeting of SF2M, Tours, France, 29-31st May 2002.

[3] Conle A, Grenier G, Johnson H, Kemp S, Kopp G, Morton M. Service history determination, SAE Fatigue Design Handbook AE-22, Society Automotive Engineers Inc, Warrendale USA, 1997, pp. 115-144.

[4] Conle A, Topper TH. Overstrain effects during variable amplitude service history testing, Int Jnl of Fatigue 1980;2(5):130-136.

[5] Austen I, Gregory R. Component test during duration prediction and acceleration by fatigue analysis and fatigue editing, VTT Symposium 1995;3(157):169-187.

[6] Stephens RI, Dindinger PM, Gunger JE. Fatigue damage editing for accelerated durability testing using strain range and SWT parameter criteria, Int Jnl of Fatigue 1997;19:599-606.

[7] Oh C-S. Application of wavelet transform in fatigue history editing, Int Jnl of Fatigue 2001;23:241-250.

[8] Giacomin J, Steinwolf A, Staszewski WJ. A vibration mission synthesis algorithm for mildly nonstationary road data, ATA 6th Int Conf on the New Role of Experimentation in the Modern Automotive Product Development Process, 17-19 Nov. 1999, Florence, Italy.

[9] Giacomin J, Steinwolf A, Staszewski WJ. An algorithm for Mildly Nonstationary Mission Synthesis (MNMS), Engineering Integrity 2000;7(January):44-56.

[10] Giacomin J, Steinwolf A, Staszewski WJ. Application of Mildly Nonstationary Mission Synthesis (MNMS) to Automotive Road Data, ATA 7th Int Conf on the New Role of Experimentation in the Modern Automotive Product Development Process, 23-25 May 2001, Florence, Italy.

[11] Abdullah S, Giacomin JA, Yates JR. A mission synthesis algorithm for fatigue damage analysis, Proc of the Instn of Mech Engrs, Part D, Journal of Automobile Engineering 2004;218(D3):243-258.

[12] Abdullah S, Yates JR, Giacomin JA. Wavelet Bump Extraction (WBE) algorithm for the analysis of fatigue damage, Proc of the 5th Int Conf on Low Cycle Fatigue (LCF5), Berlin, Germany, 9-11th September 2003, pp 445-450.

[13] Conle A, Landgraf R. A fatigue analysis program for ground vehicle components, Proc of Int Conf on Digital Techniques in Fatigue, London, 1983, pp 1-28.

[14] Wu WF, Liou HY, Tse HC. Estimation of fatigue damage and fatigue life of components under random loading, Int Jnl of Pres Ves & Piping 1997; 72:243-249.

[15] Fatemi A, Yang L. Cumulative fatigue damage and life prediction theories: a survey of the state of the art for homogeneous materials, Int Jnl of Fatigue 1998;20(1):9-34.

[16] Liou HY, Wu WF, Shin CS. A modified for the estimation of fatigue life derived from random vibration theory, Probabilistic Engineering Mechanics 1999;14:281-288.

[17] Marco SM, Starkey WL. A concept of fatigue damage, Transaction of the ASME 1954;76:627-632.

[18] Taheri F, Trask D, Pegg N. Experimental and analytical investigation of fatigue characteristics of 350WT steel under constant and variable amplitude loading, Marine Structures 2003;16:69-91.

[19] DuQuesnay DL, Pompetzki MA, Topper TH. Fatigue life prediction for variable amplitude strain histories, SAE Transactions (SAE930400) 1993;102(5):455-465.

[20] Vormwald M, Seeger T. The consequences of short crack closure on fatigue crack growth under variable amplitude loading, Fatigue Fract Eng Mater Struct 1991;14(3):205-225.

[21] Bendat JS, Piersol AG. Random Data: Analysis and Measurement Procedures, 2nd Edition, Wiley-Interscience, New York, 1986.

[22] Matlab User's Guide, Matlab 5.2, The Math Works, 1998.

[23] Newland DE. An Introduction to Random Vibrations Spectral and Wavelet Analysis, 3rd Edition, Longman Scientific and Technical, New York, 1993.

[24] Daubechies I. Ten Lectures on Wavelets, SIAM, Philadelphia, 1992.

[25] Staszewski WJ. Wavelet based compression and feature selection for vibration analysis, Journal of Sound and Vibration 1998;211(5):735-760.

[26] Barclay VJ, Bonner RF. Application of wavelet transforms to experimental spectra: smoothing, denoising and data set compression, Analytical Chem 1997;69:78-90.

[27] Steinwolf A, Giacomin J, Staszewski WJ. On the need for bump event correction in vibration test profiles representing road excitations in automobiles, Proc of the Instn of Mech Engrs, Part D, Journal of Automobile Engineering 2002;216(D4):279-295.

[28] Hubbard BB. The World According to Wavelets, A K Peters, Massachusetts USA, 1996.

[29] ASTM E606-92, Standard practice for strain-controlled fatigue testing, American Society for Testing and Materials, 1998.

[30] DuQuesnay DL. Applications of overload data to fatigue analysis and testing, Application of Automation Technology in Fatigue and Fracture Testing and Analysis: Fourth Volume, ASTM STP 1411, edited by Braun AA, McKeighan PC, Nicolson AM, Lohr RD. ASTM, West Conshohocken USA, 2002, pp 165-180.

[31] Topper TH, Lam TS. Effective strain-fatigue life data for variable amplitude loading, Int Jnl of Fatigue 1997;19(Supp No.1):S137-S143.

[32] Khalil M, Topper TH. Prediction of crack-opening stress levels for 1045 as-received steel under service loading spectra, Int Jnl of Fatigue 2003;25:149-157.

[33] Khalil M, DuQuesnay DL, Topper TH. Prediction of crack-opening stress levels for service loading spectra, Application of Automation Technology in Fatigue and Fracture Testing and Analysis: Fourth Volume, ASTM STP 1411, edited by Braun AA, McKeighan PC, Nicolson AM, Lohr RD. ASTM, West Conshohocken USA, 2002, pp 165-180.

[34] Matsuishi M, Endo T. Fatigue of metals subjected to varying stress, Proc of the Kyushu Branch of Japan Society of Mechanics Engineering, Fukuoka, Japan, 1968, pp 37-40.

[35] nSoft® User Manual, nCode International Ltd, Sheffield, 2001.

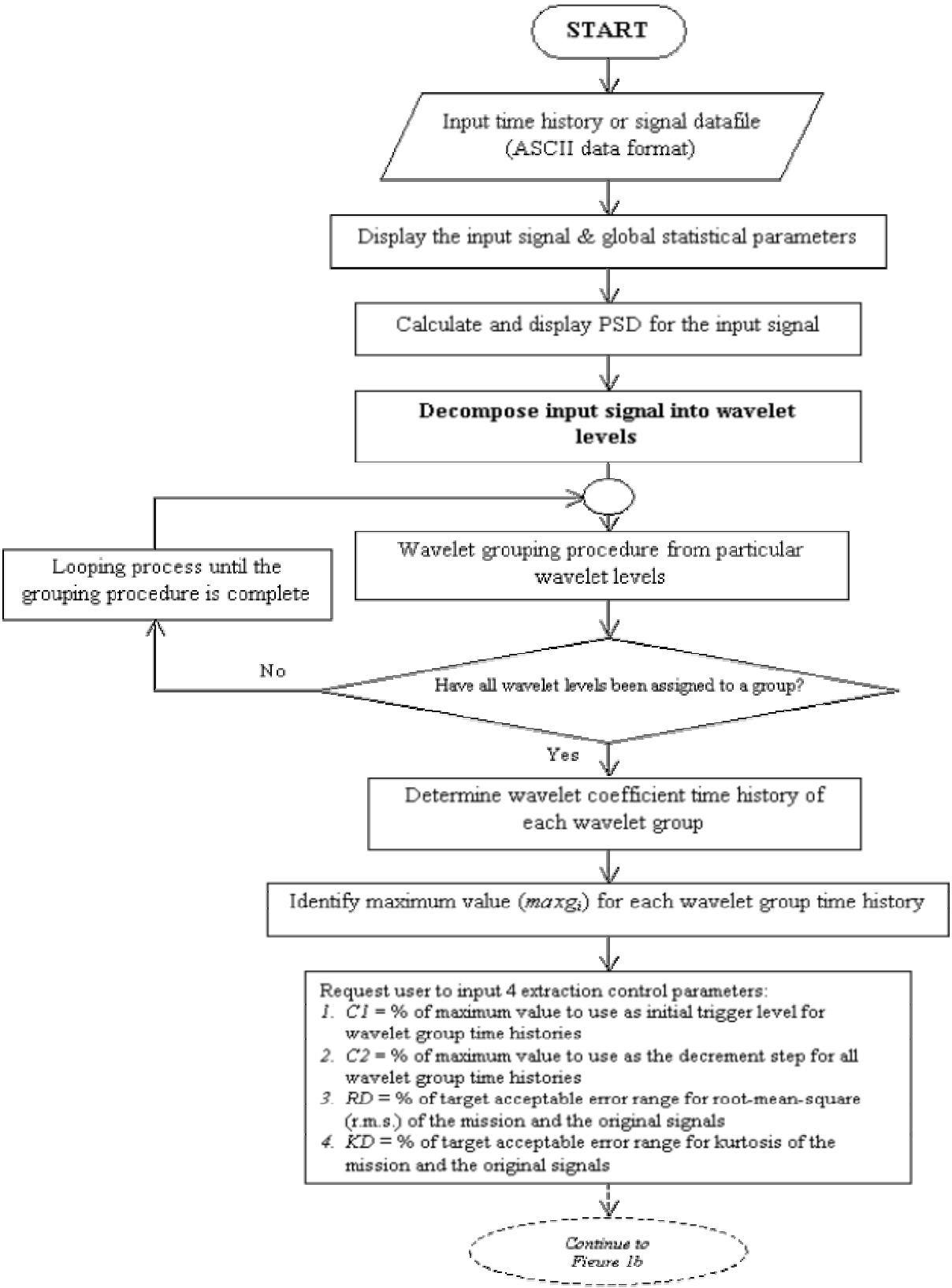

Fig. 1. The WBE algorithm flowchart: (a) Stage 1 - wavelet decomposition and grouping stages.

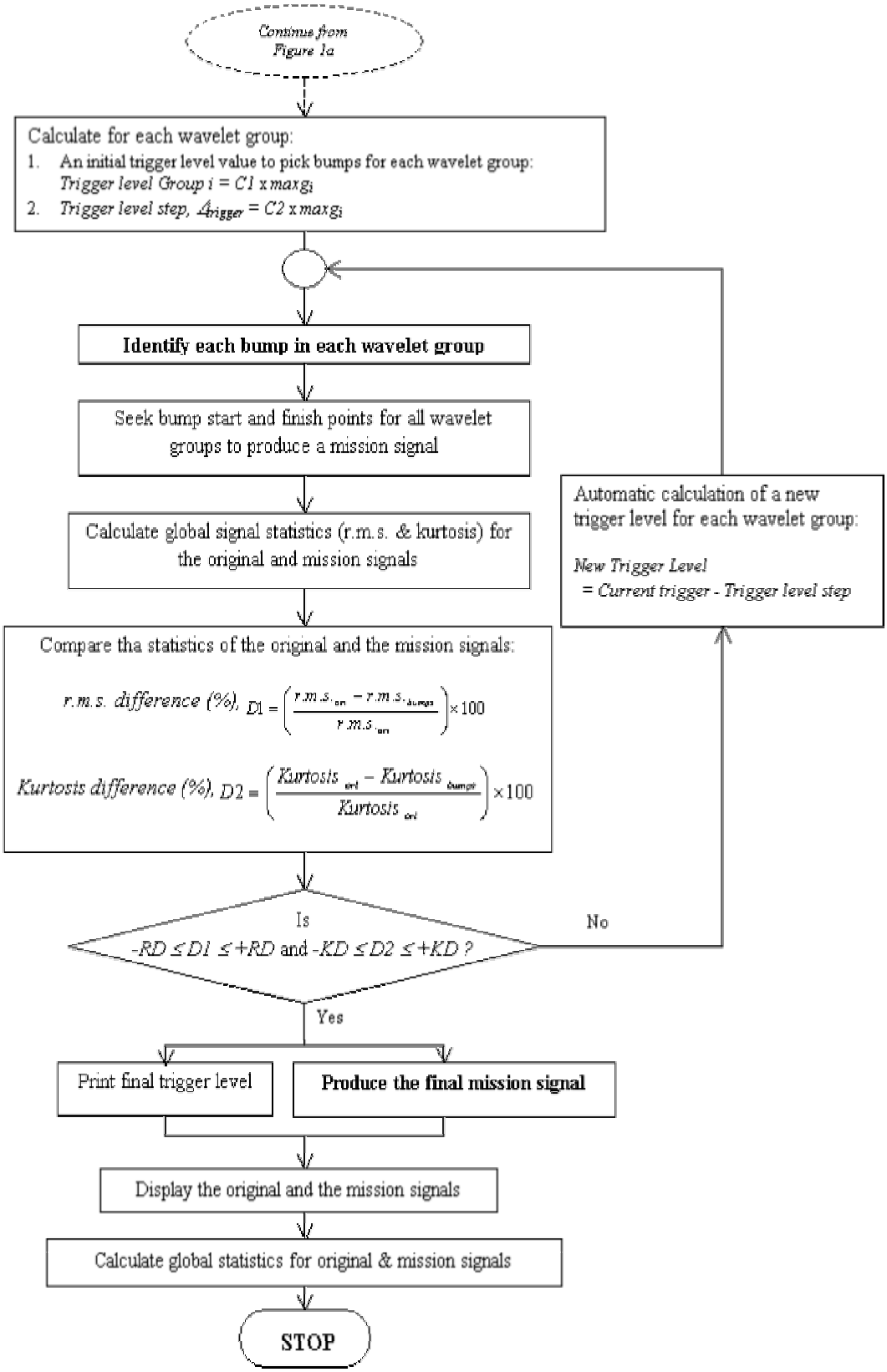

Fig. 1. The WBE algorithm flowchart: (b) Stage 2 – identification and extraction of fatigue damaging events, and production of the mission signal.

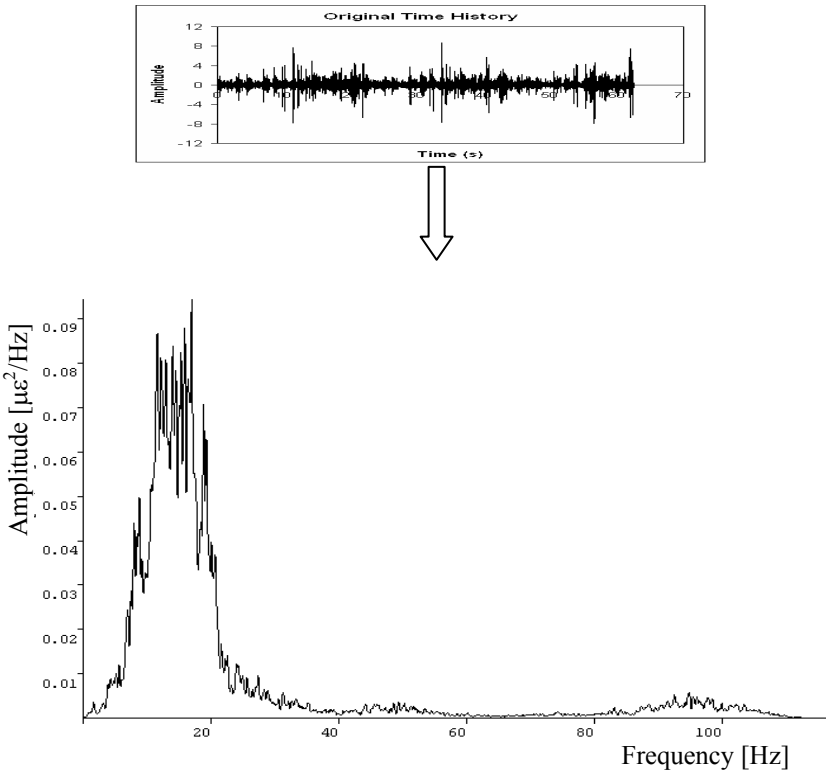

Fig. 2. An example of a variable amplitude loading and its power spectral density plot.

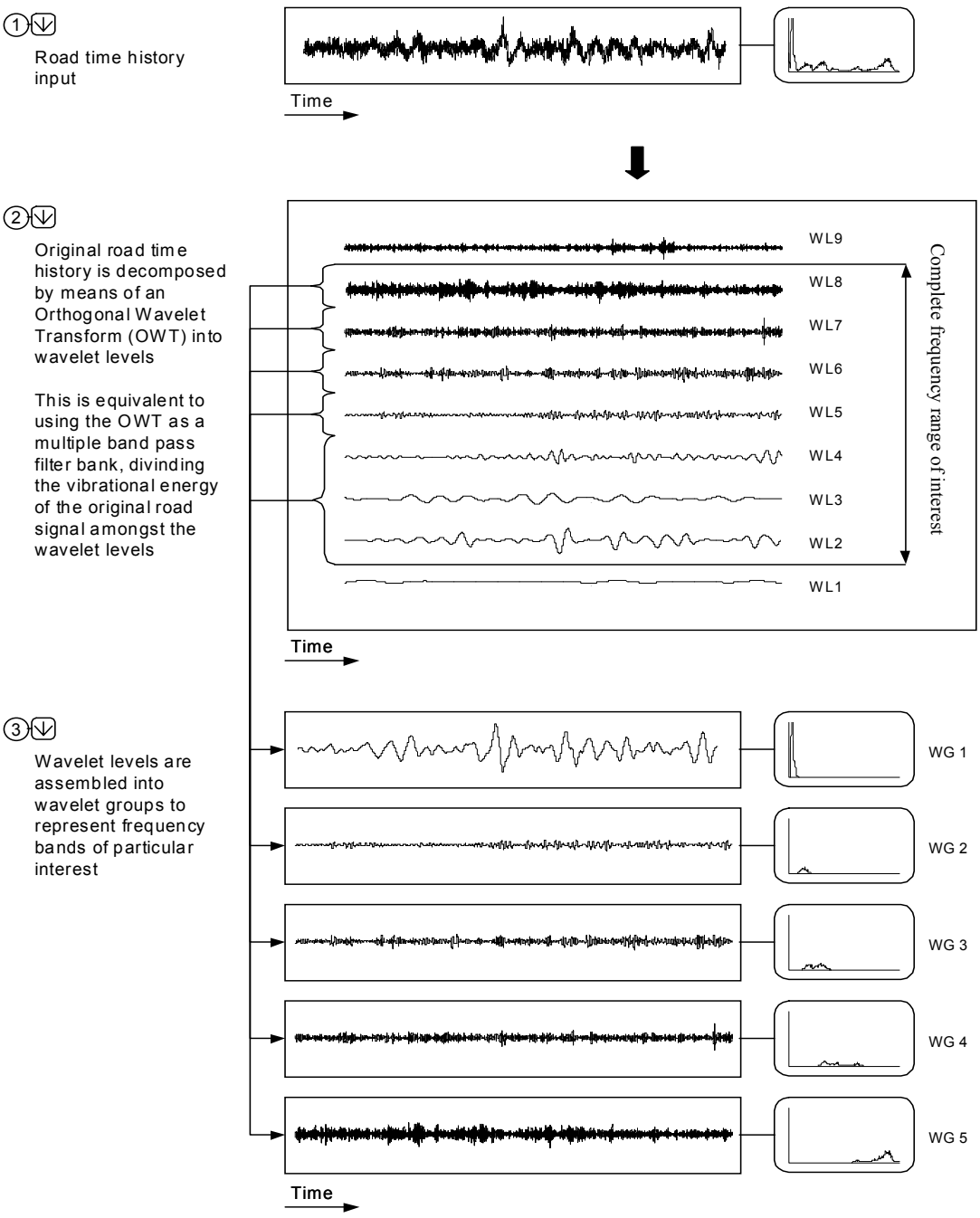

Fig. 3. Schematic diagram of the wavelet decomposition and grouping procedure for a variable amplitude loading, where WL and WG denoted as wavelet level and wavelet group, respectively.

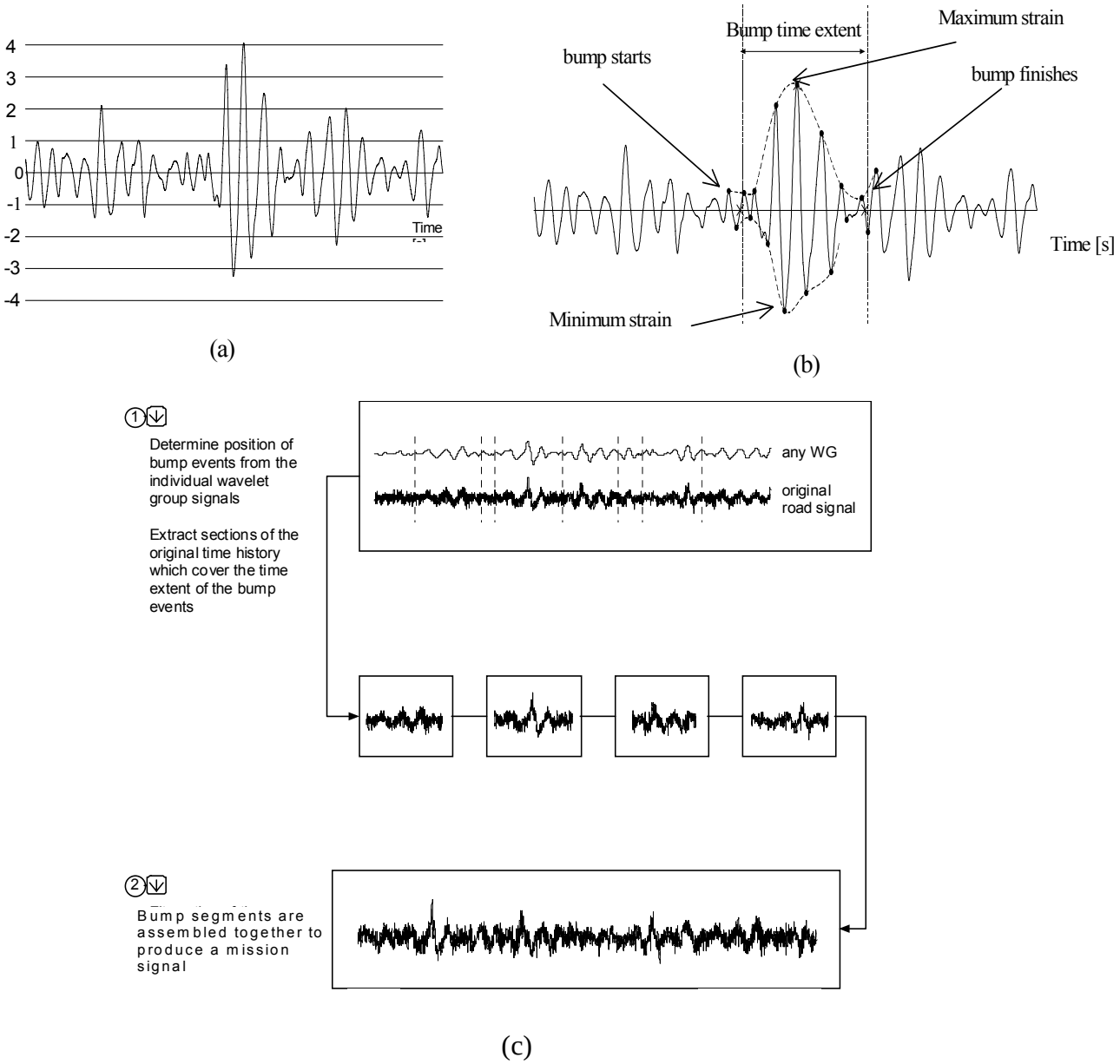

Fig. 4. Bump identification and the production of a mission signal: (a) Bump identification using trigger levels, (b) Decay enveloping of a bump event, (c) Seeking the bump start and finish points.

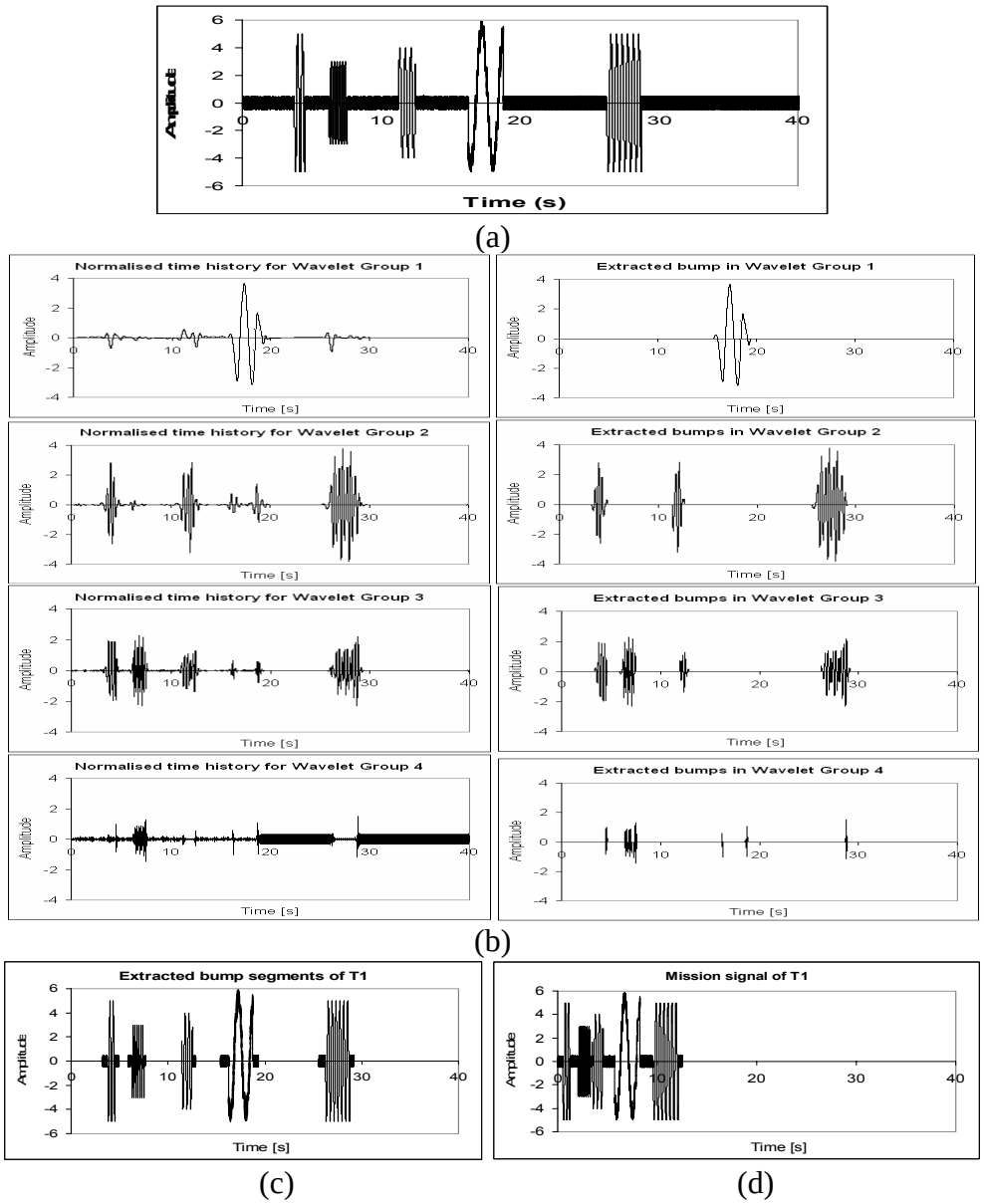

Fig. 5. Time history plots for T1: (a) The original time history, (b) Time histories in normalised scale of the wavelet groups and the location of bumps in the respective wavelet group, (c) The extracted bump segments at their original time positions, (d) The mission time history.

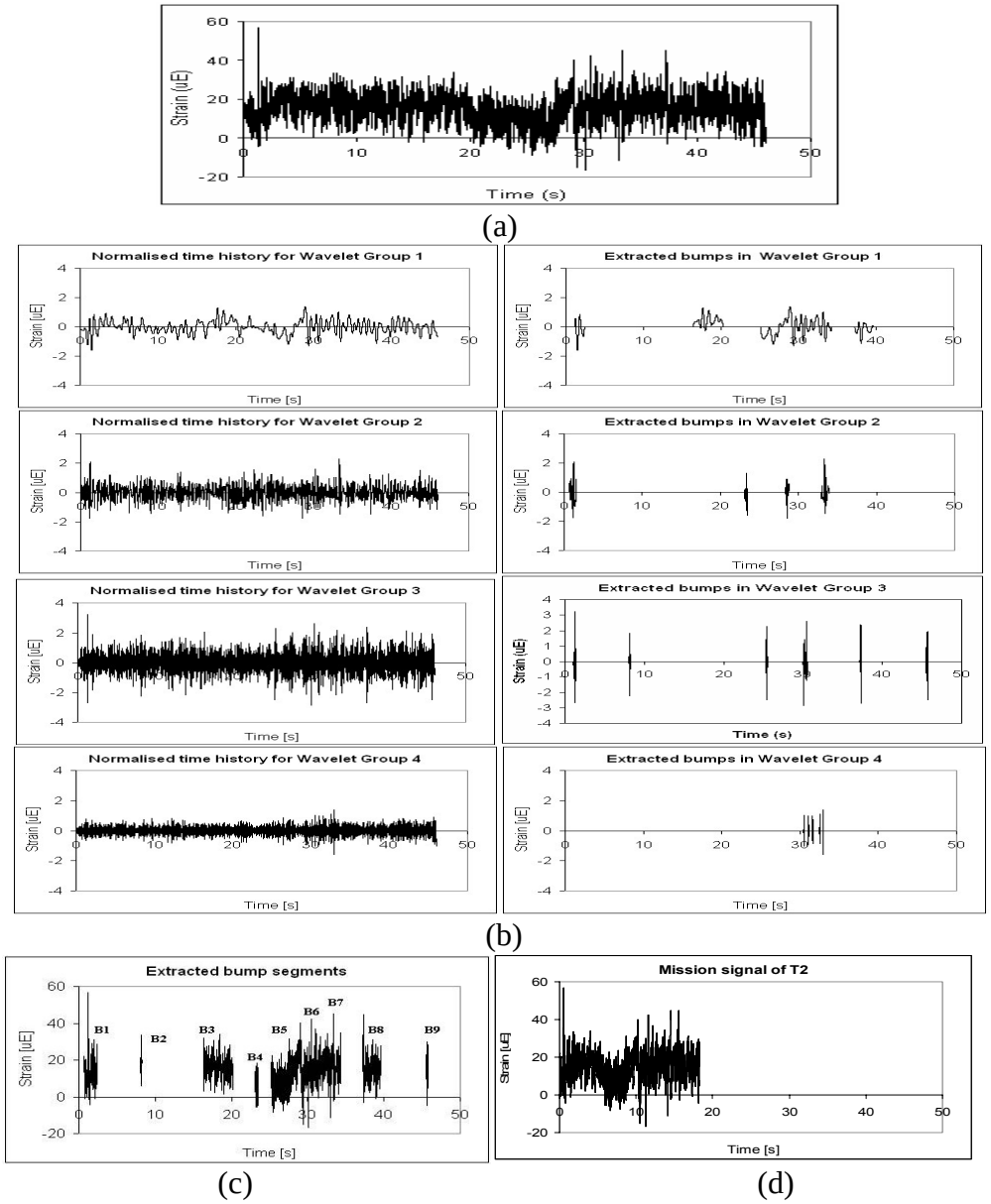

Fig. 6. Time history plots for T2: (a) The original time history, (b) Time histories in normalised scale of the wavelet groups and the location of bumps in the respective wavelet group, (c) The extracted bump segments at their original time positions where B1 – B9 denoted as the number of bump segment**,** (d) The mission time history.

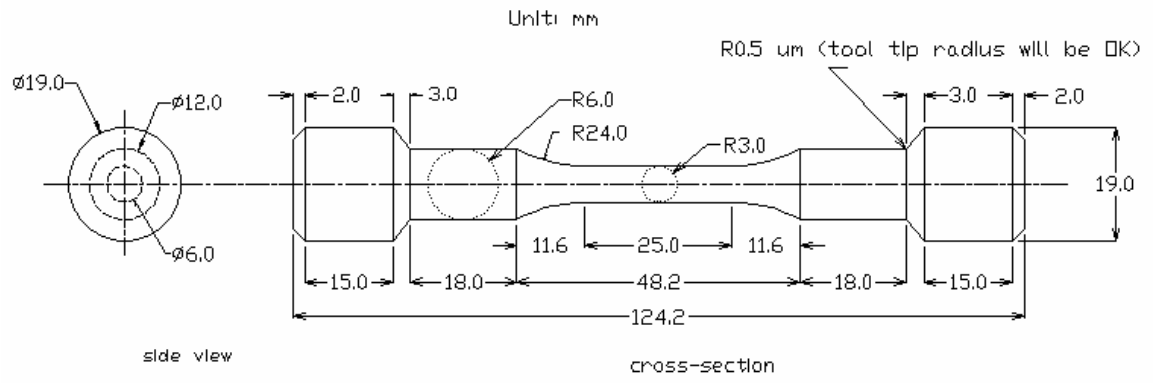

(a)

(b)

Fig. 7. Experimental set-up: (a) The geometry and dimensions of the specimen - all in the unit of mm unless specified, (b) A specimen at the servo-hydraulic machine with a 25-mm extensometer.

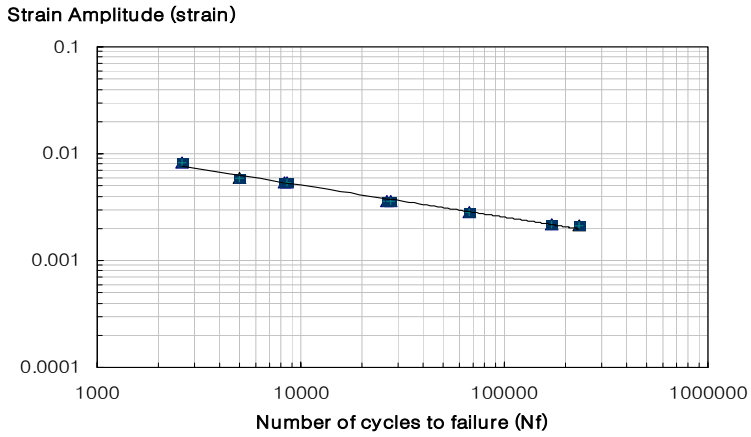

(a)

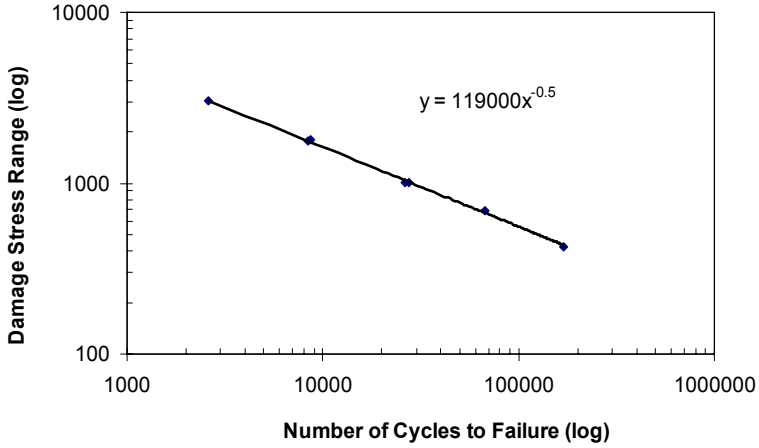

(b)

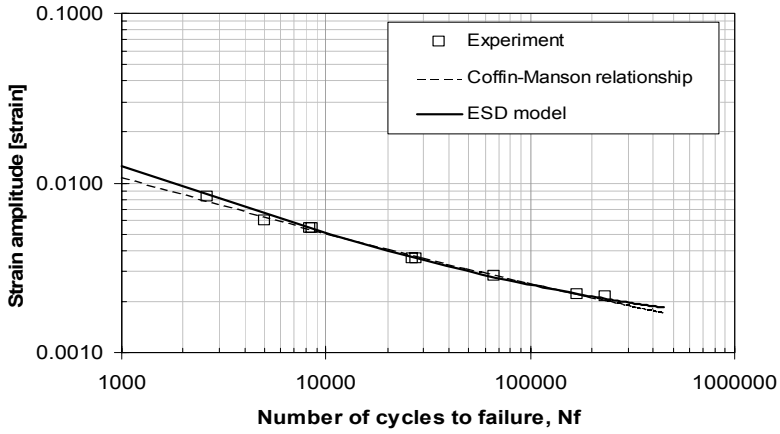

(c)

Fig. 8. (a) The curves obtained from experiments: CA loading strain-life curve. (b) The graph of $E\Delta\varepsilon^{*}$ versus fatigue life using the CA loading fatigue data. (c)Comparison between the ESD, Coffin-Manson strain-life curves and the experimental strain-life points.

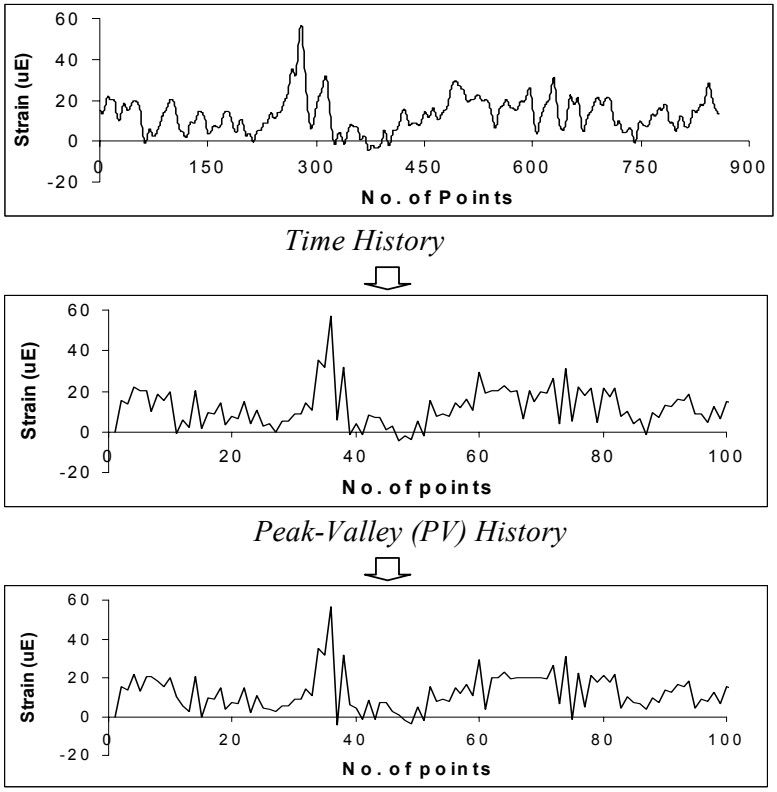

Fig. 9 Order of cycle history for the first bump segment (B1) of T2.

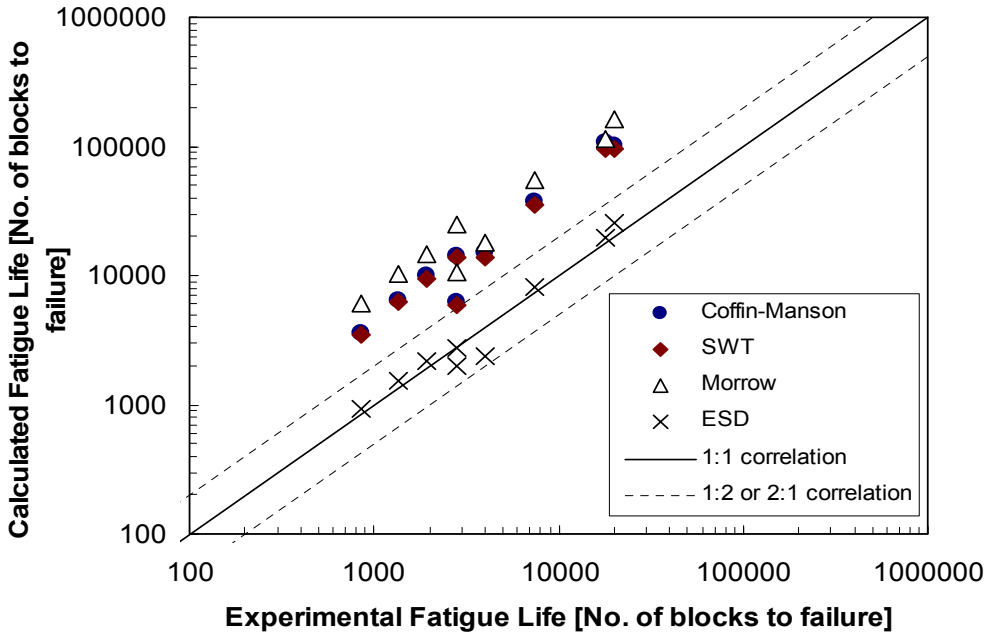

Fig. 10. Fatigue lives correlation of the nine bump segments between prediction methods and experimental results.

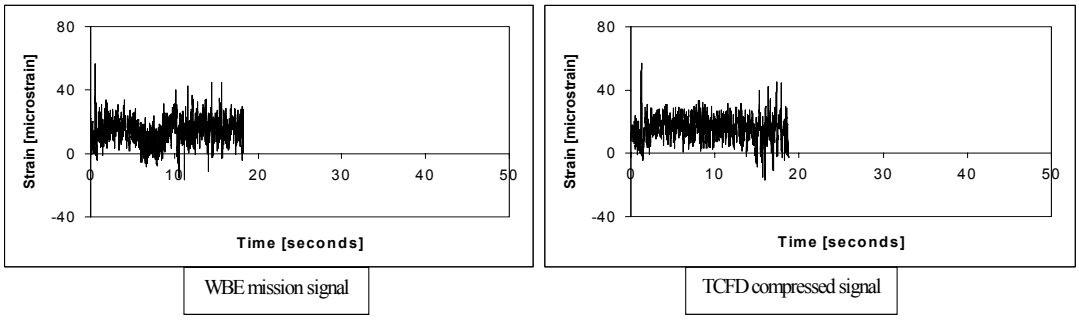

(a)

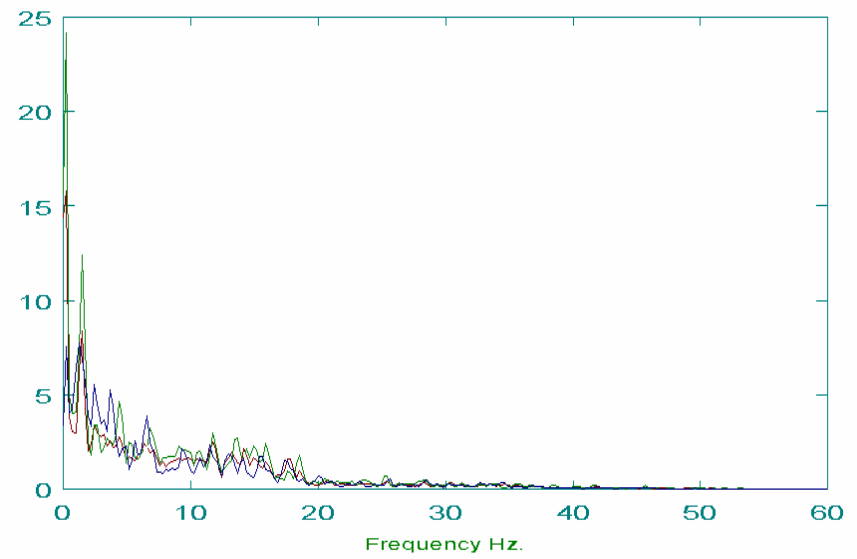

(b)

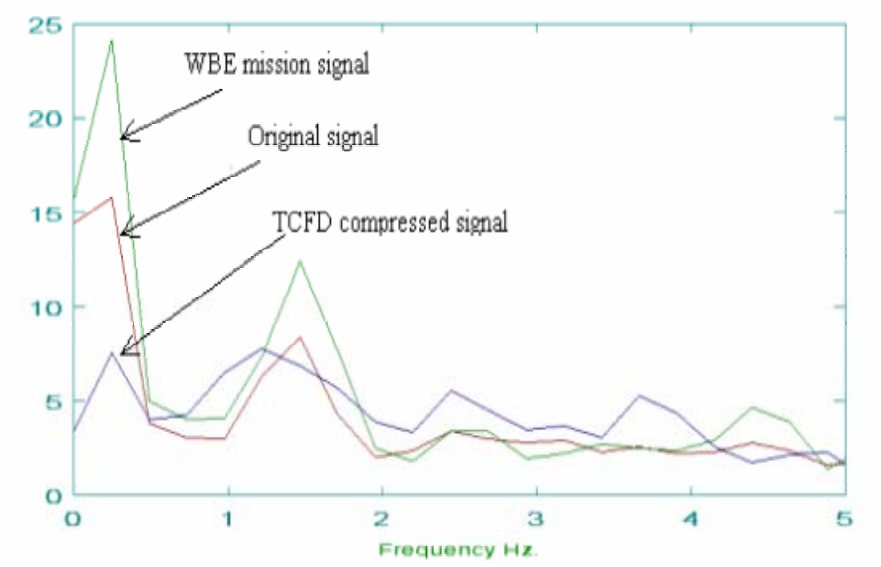

(c)

Fig. 11. (a) The WBE mission signal and TCFD compressed signal, (b) PSD comparison in the frequency range of 0-60 Hz, (b) PSD comparison in the frequency range of 0-5 Hz.

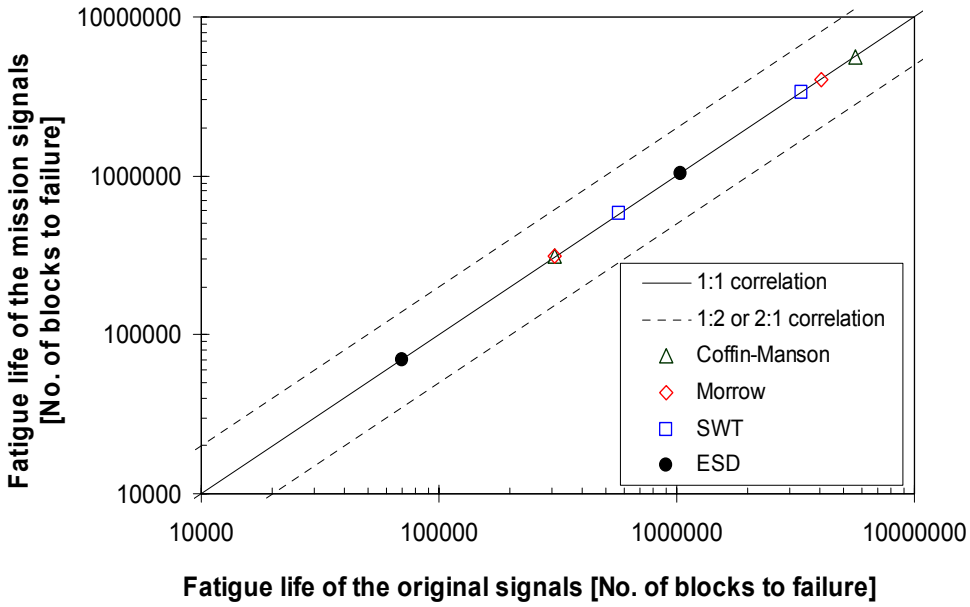

Fig. 12. Correlation between the mission and the original signals of T1 and T2 using four strain-life models.

Table 1

Mechanical properties of BS 080A42 steel determined from the tensile test and CA loading fatigue tests.

Monotonic Properties		Cyclic Propertiesof the Coffin-Manson equation	
Ultimate tensile strength, S_u [MPa]	624	Fatigue strength coefficient, σ'_f [MPa]	1505
Modulus of elasticity, E [GPa]	210	Fatigue strength exponent, b	-0.144
Static yield stress 0.2%, S_y [MPa]	342	Fatigue ductility coefficient, ε'_f	0.176
Area reduction, (%)	51.9	Fatigue ductility exponent, c	-0.400
Elongation (%)	28.4		

Table 2

Identification of T2 bump segments (refer to Fig. 6c for the time histories).

Signal Name	Signal length [s]	Position in the original signal	
		Start time [s]	End time [s]
B1	1.7	0.68	2.39
B2	0.2	8.07	8.25
B3	3.9	16.32	20.21
B4	0.5	23.07	23.53
B5	2.4	25.14	27.50
B6	4.6	27.50	32.06
B7	2.3	32.07	34.34
B8	2.5	37.14	39.65
B9	0.3	45.47	45.77

Table 3

Fatigue lives of the original and the mission signals of T2 at several values of the α and β values using a carbon steel or SAE 1045 steel.

Reference	α	β	Fatigue life [no. of blocks to failure]	
			T2	T2-mission
DuQuesnay *et al.* 1993 [19]	0.45	0.8	178	204
Topper and Lam 1997 [31]	0.75	0.23	178	204
Khalil and Topper 2003 [32]	0.55	0.23	178	204

Table 4

Fatigue lives of the T2 bump segments obtained from experiments and predictions.

Segment	Fatigue Life [Number of blocks to failure]				
	Experiment	Coffin-Manson	Morrow	SWT	ESD
B1	2831	5964	10462	10462	1968
B2	17880	97000	114000	114000	19523
B3	3996	14008	17720	17720	2400
B4	20084	96400	163000	163000	25586
B5	2792	13708	24566	24566	2714
B6	843	3428	6070	6070	927
B7	1366	6216	10409	10409	1536
B8	1942	9370	14783	14783	2206
B9	7500	35667	55200	55200	8181
T2	191	642	1194	665	178
T2-mission	319	1057	2013	1092	204

Table 5

Comparison of the signal statistics and fatigue lives between the original, WBE mission and TCFD compressed signals.

Signal	Signal length [seconds]	Signal Statistics	
		r.m.s.	kurtosis
Original Signal	46.0	16.7	3.4
WBE mission signal	18.8	16.6	3.6
TCFD compressed signal	18.8	17.4	4.1

Table5

The compression characteristics between the original and mission signals.

Signal Name		Signal Identification		Signal Statistics			Fatigue Life Prediction (ESD model)	
		Signal length [s]	Time ratio [%]	r.m.s.	Kurtosis	WBE required difference	Fatigue life [blocks to failure]	Fatigue Life ratio [%]
T1	Original signal	40.0		1.5	7.4		69930	
	Mission signal	12.5	31.3	2.6	2.5	±75.0%	69930	100
T2	Original signal	46.0		16.7	3.4		1035240	
	Mission signal	18.8	40.9	16.6	3.6	±10.0%	1035240	100

Note: *Time ratio (%) = ($t_{mission}$ / $t_{original}$) x 100%; Damage Ratio (%) = ($D_{mission}$ / $D_{original}$) x 100%*